


Generation of cat states by a weak parametric drive and a transitionless tracking algorithmShuai Liu,^{1,2,3,*} Ye-Hong Chen,^{4,5,1,2,*} Yu Wang,^{1,2} Yi-Hao Kang⁶, Zhi-Cheng Shi,^{1,2} Jie Song,⁶ and Yan Xia^{1,2,†}¹*Fujian Key Laboratory of Quantum Information and Quantum Optics (Fuzhou University), Fuzhou 350116, China*²*Department of Physics, Fuzhou University, Fuzhou 350116, China*³*School of Physics and Electronic Engineering, Hubei University of Arts and Science, Xiangyang 441053, China*⁴*Theoretical Quantum Physics Laboratory, RIKEN Cluster for Pioneering Research, Wako-shi, Saitama 351-0198, Japan*⁵*RIKEN Center for Quantum Computing (RQC), 2-1 Hirosawa, Wako-shi, Saitama 351-0198, Japan*⁶*Department of Physics, Harbin Institute of Technology, Harbin 150001, China*

(Received 18 February 2022; accepted 4 October 2022; published 20 October 2022)

In this paper, we present an experimentally feasible protocol to generate the cat states in the microwave resonator coupled to a superconducting qubit. The setup employs a detuned, time-dependent parametric drive to squeeze the resonator mode so that an adjustable qubit-resonator coupling strength can be obtained. Therefore, based on the transitionless tracking algorithm, we can design control pulses to generate the qubit-resonator entangled states with high fidelity in the laboratory frame. Then, the even and odd cat states can be further obtained by performing measurement on the superconducting qubit. Compared to the scheme [Chen *et al.*, *Phys. Rev. Lett.* **126**, 023602 (2021)], the present protocol is realized in the regime of weak parametric drive. In the case, squeezing-induced noise can be reduced so that the fidelity of the generated state can be improved. Numerical simulations indicate that the present protocol is well executed under experimentally available parameters. Thus, the protocol is feasible with the present state of the art in microwave superconducting circuits.

DOI: [10.1103/PhysRevA.106.042430](https://doi.org/10.1103/PhysRevA.106.042430)**I. INTRODUCTION**

Superconducting quantum circuits, providing an ideal platform in the fields of quantum information, quantum computation, and quantum simulation [1–17], have received extensive attention. These solid-state circuits show excellent properties for realizing quantum coherent interactions with high sufficiently controllability and scalability [18,19]. To date, remarkable progress has been made towards improving the qubit coherence and circuit complexity [20–24]. In addition, the long coherence time of superconducting resonators has been demonstrated in recent experiments [25,26]. Due to these advantages, many schemes have been proposed to generate kinds of nonclassical states of superconducting resonators [9], for instance, Fock states [27,28], cat states [29–31], and arbitrary quantum superposition states [32].

Among the above nonclassical states [27–32], cat states [33] formed by the superpositions of two coherent states with the same amplitudes but opposite phases, are one of important nonclassical states. In general, cat states with large sizes not only provide the test of the fundamentals of quantum physics [34,35], but also have extensive applications in modern quantum technologies, such as quantum information processing and quantum metrology [36–42]. For example, cat states with large sizes can be utilized as qubits against photon dephasing [43]. Therefore, they are very promising for the fault-tolerant quantum computation [44–46]. However, high-

fidelity preparation of cat states is still challenging because of their sensitivity to photon loss. For example, Leroux *et al.* adiabatically prepared the cat states in the squeezed-light frame [31]. In the scheme, the change in control parameters must be slow to meet the adiabatic limit in the adiabatic control, which usually leads to a long-time evolution. Such a long-evolution time inevitably aggravates the effect of dissipation on the fidelity of target state because decoherences, noises, or losses would spoil the intended dynamics. Therefore, shortening the evolution time by accelerating the system dynamics towards the target states can reduce the influence of the decoherences, noises, or losses on the fidelity of the final cat states [47].

To realize the fast, robust, high fidelity, and reliable generation of the cat states, some researchers have suggested using the shortcuts-to-adiabatic (STA) methods [48–56] to speed up the evolution process. The basic idea of the STA method is mimicking adiabatic dynamics beyond the adiabatic limit to achieve rapid system evolution [57–71]. Until now, several protocols have been proposed for the generation of cat states by STA methods [72–74]. For example, following the proposal by Leroux *et al.* [31], Chen *et al.* exploited a parametric amplification to generate the cat states via STA dynamics [74]. In the scheme, the strong light squeezing is necessary to generate the cat states. However, it is still a challenge to generate strong parametric drives with current experimental technology. Besides, the strong squeezing of the resonator mode can excite the squeezing-resonator mode and cause significant squeezing-induced noise [75–80]. Such noise will reduce the fidelity of the generated cat states.

In this paper, to overcome the flaw of the scheme in Ref. [74], we propose a protocol to generate the cat states

*These authors contributed equally to this work.

†xia-208@163.com

using a weak parametric drive inside a resonator. In the protocol, the effective Rabi Hamiltonian is obtained by suppressing the undesired interaction terms using the external classical driving field on the qubit. Then, by constructing a STA passage with a transitionless tracking algorithm [49], the cat states can be accurately generated along the instantaneous eigenstate of the Rabi Hamiltonian. By performing measurement on the superconducting qubit, the microwave resonator collapses to the even or odd cat states. Note that the idea of adding external classical driving field on the qubit originates from the paper [74]. However, we present an extensive theoretical analysis of this idea and propose an experimentally feasible protocol to generate the cat states in the microwave resonator in the regime of weak parametric drive. Compared to the scheme in Ref. [74], the required squeezing intensity in the current protocol is significantly decreased at the expense of an increased physical coupling strength between the qubit and the resonator. As is well known, it is easier for experiments to realize a strong classical drive than a strong parametric drive. Therefore, the current protocol can be easier realized compared to the one in Ref. [74]. Moreover, because a strong squeezing of the resonator mode causes significant noise to the system [74,76–80] to suppress the influence of such noise, it usually needs to couple the system to squeezing-vacuum reservoirs in the previous schemes [74,76–80]. In the present paper, the squeezing-induced noise is negligible due to the weak parametric drive. Thus, compared to the previous schemes in Refs. [74,76–80], the present protocol does not require a squeezing-vacuum reservoir, which reduces the experimental complexity. Additionally, numerical simulations indicate that the present protocol is well executed under experimentally available parameters.

The outline of the paper is as follows. In Sec. II, we present the physical model of the system and derive the effective Hamiltonian. In Sec. III, we show the generation of the cat states in the regime of weak parametric drive by transitionless tracking algorithm. In Sec. IV, we analyze the influence of single-photon loss and leakage to the excited state on the present protocol by numerical simulations. Finally, the discussions and conclusions are presented in Sec. V.

II. PHYSICAL MODEL AND HAMILTONIAN

As illustrated in Fig. 1(a), we consider a superconducting qubit-resonator coupled system. The corresponding level configuration of the superconducting qubit is shown in Fig. 1(b). The superconducting resonator can be a transmission line resonator or a coplanar waveguide resonator; and the superconducting qubit can be a transmon or flux qubits [6,7]. The free Hamiltonian describing the superconducting qubit and the resonator mode is given by ($\hbar=1$, hereafter)

$$H_q = \frac{\omega_q}{2} \sigma_z + \omega_c a^\dagger a, \quad (1)$$

where $\sigma_z = |e\rangle\langle e| - |g\rangle\langle g|$, ω_q is the energy gap between the ground-state $|g\rangle$ and the excited state $|e\rangle$ of the superconducting qubit, a (a^\dagger) is the annihilation (creation) operator of the resonator mode, and ω_c is the associated resonance frequency of the fundamental mode of the resonator.

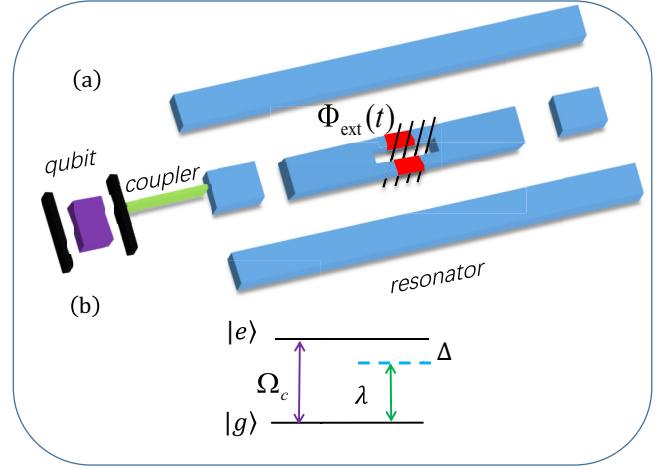


FIG. 1. Schematic illustration of the protocol. (a) A superconducting resonator embedded with a superconducting quantum interference device (SQUID) loop is coupled to a superconducting qubit. The parametric drive of the resonators $\Omega_1(t)$ and $\Omega_2(t)$ can be realized by modulating an external magnetic flux $\Phi_{\text{ext}}(t) = \Phi_{\text{ext1}}(t) + \Phi_{\text{ext2}}(t)$, where $\Phi_{\text{ext1}}(t)$ and $\Phi_{\text{ext2}}(t)$ are the components of the flux $\Phi_{\text{ext}}(t)$ and have a phase difference of $\pi/2$. (b) The level configuration of superconducting qubit. Here, the superconducting qubit is coupled to the resonator with coupling strength λ and detuning Δ and is driven by the classical field with Rabi frequency Ω_c .

The bare interaction of the qubit-resonator system can be described by

$$H_I = \lambda(a + a^\dagger)\sigma_x, \quad (2)$$

where $\sigma_x = |e\rangle\langle g| + |g\rangle\langle e|$, and λ denotes the coupling strength between the superconducting qubit and the resonator. When $\lambda/\omega_q \ll 1$ and $\lambda/\omega_c \ll 1$, under the rotating-wave approximation, the Hamiltonian in Eq. (2) is reduced to the extensively studied Jaynes-Cummings model by neglecting the fast-oscillating terms,

$$H_{JC} = \lambda a |e\rangle\langle g| + \text{H.c.} \quad (3)$$

In addition, the superconducting resonator is subjected to two time-dependent parametric drives with the same frequency ω_p and different real amplitudes $\Omega_1(t)$ and $\Omega_2(t)$. It is worth emphasizing that the two drives $\Omega_1(t)$ and $\Omega_2(t)$ have a phase difference of $\pi/2$. As shown in Fig. 1(a), the parametric drive of the resonator can be implemented by modulating the flux $\Phi_{\text{ext}}(t) = \Phi_{\text{ext1}}(t) + \Phi_{\text{ext2}}(t)$ threading the resonator-embedded SQUID loop in the middle of the transmission line [81–85], where $\Phi_{\text{ext1}}(t)$ and $\Phi_{\text{ext2}}(t)$ are the components of the flux $\Phi_{\text{ext}}(t)$ and have a phase difference of $\pi/2$. Additionally, a classical driving field with amplitude Ω_c and frequency ω_l is imposed on the superconducting qubit to drive the transition between $|e\rangle$ and $|g\rangle$.

A direct result of parametric drives for the superconducting resonator is that it will lead to an exponentially enhanced qubit-resonator interaction [31,74–80]. A possible physical implementation of parametric drives is also shown in the Appendix. To be more specific, the whole Hamiltonian of the

model is represented as

$$H(t) = \omega_c a^\dagger a + \frac{\omega_q}{2} \sigma_z + \left[\frac{\Omega_c}{2} e^{-i\omega_l t} |e\rangle\langle g| + \lambda a^\dagger |g\rangle\langle e| - \frac{\Omega_1(t) + i\Omega_2(t)}{2} a^2 e^{i\omega_p t} + \text{H.c.} \right]. \quad (4)$$

To work out the effective Hamiltonian, in a proper observation frame at $\omega_p/2$, the Hamiltonian $H(t)$ in Eq. (4) reads

$$H_r(t) = \Delta a^\dagger a + \frac{\Omega_c}{2} \sigma_x + \left[\lambda a^\dagger |g\rangle\langle e| - \frac{\Omega_1(t) + i\Omega_2(t)}{2} a^2 + \text{H.c.} \right], \quad (5)$$

where $\Delta = \omega_c - \omega_p/2$, and we have assumed $\omega_q = \omega_l = \omega_p/2$. Then, we further perform a squeezing transformation $S(t) = \exp[r(t)(a^2 - a^{\dagger 2})/2]$ on the Hamiltonian $H_r(t)$ in Eq. (5), where $r(t)$ is a real squeezing parameter satisfying $\tanh[2r(t)] = \Omega_1(t)/\Delta$. In the squeezing frame determined by $S(t)$, the Hamiltonian $H_r(t)$ in Eq. (5) is derived into the following terms in the squeezed frame,

$$\begin{aligned} H_s(t) &= S^\dagger(t) H_r(t) S(t) + i\dot{S}^\dagger(t) S(t) \\ &= H_{\text{Rabi}}(t) + H_{\Omega_c} + H_{\text{err1}}(t) + H_{\text{err2}}(t), \\ H_{\text{Rabi}}(t) &= \Delta \operatorname{sech}[2r(t)] a^\dagger a + \lambda e^{r(t)} \sigma_x (a^\dagger + a)/2, \\ H_{\Omega_c} &= \frac{\Omega_c}{2} \sigma_x, \\ H_{\text{err1}}(t) &= -i\lambda e^{-r(t)} \sigma_y (a^\dagger - a)/2, \\ H_{\text{err2}}(t) &= [\Omega_2(t) - i\dot{r}(t)](a^{\dagger 2} - a^2)/2, \end{aligned} \quad (6)$$

with $\sigma_y = i(|g\rangle\langle e| - |e\rangle\langle g|)$. The term $H_{\text{Rabi}}(t)$ represents the Rabi interaction between the superconducting qubit and the resonator. The term H_{Ω_c} describes a σ_x driving interaction on the qubit. The remaining terms $H_{\text{err1}}(t)$ and $H_{\text{err2}}(t)$ describe undesired corrections for the ideal Rabi Hamiltonian $H_{\text{Rabi}}(t)$, which need to be suppressed or eliminated. Obviously, the term $H_{\text{err2}}(t)$ can be naturally eliminated by choosing $\Omega_2(t) = i\dot{r}(t)$. The term $H_{\text{err1}}(t)$ can be suppressed by the additional classical driving field Ω_c . It is worth noting that the additional classical driving field Ω_c on the qubit is important in the present protocol, which is different from the scheme [74]. Without the classical drive Ω_c , the term $H_{\text{err1}}(t)$ needs to be canceled by using a large $\Omega_1(t)$. To illustrate the reason, we move to the rotating frame with respect to $U_x(t) = \exp(-iH_{\Omega_c}t)$ so that the Hamiltonian $H_s(t)$ is transformed to

$$\begin{aligned} H'_s(t) &= H_{\text{Rabi}}(t) + H'_{\text{err1}}(t), \\ H'_{\text{err1}}(t) &= i \frac{\lambda e^{-r(t)}}{2} [\cos(\Omega_c t) \sigma_y - \sin(\Omega_c t) \sigma_z] (a - a^\dagger) \\ &= \frac{\lambda e^{-r(t)}}{4} [i(e^{i\Omega_c t} + e^{-i\Omega_c t}) \sigma_y - (e^{i\Omega_c t} - e^{-i\Omega_c t}) \sigma_z] (a - a^\dagger). \end{aligned} \quad (7)$$

When $\Omega_c \gg \lambda e^{-r(t)}/4$, the Hamiltonian $H'_{\text{err1}}(t)$ can be neglected as a fast-oscillating term. Therefore, the effective Hamiltonian of the system becomes

$$H_{\text{eff}}(t) \approx H'_s(t) \approx \Delta \operatorname{sech}[2r(t)] a^\dagger a + \lambda_s(t) \sigma_x (a^\dagger + a)/2, \quad (8)$$

with an exponentially enhanced interaction strength $\lambda_s(t) = \lambda e^{r(t)}/2$.

III. GENERATING THE CAT STATES IN THE REGIME OF THE WEAK PARAMETRIC DRIVE

In this section, we focus on the generation of a large-size cat state in the regime of a weak parametric drive by the shortcuts-to-adiabatic (STA) method.

A. The ground state of the effective Hamiltonian

For the effective Hamiltonian $H_{\text{eff}}(t)$ in Eq. (8), the qubit-resonator interaction acts as a time-dependent σ_x -dependent linear force on the resonator. This force drives the resonator into one of two coherent states $|\pm \alpha(t)\rangle$ $\{\alpha(t) = \lambda_s(t)/\Delta \operatorname{sech}[2r(t)]\}$, conditioned on the state of the qubit in the σ_x basis [86]. In this case, the effective Hamiltonian $H_{\text{eff}}(t)$ in Eq. (8) can be diagonalized by the unitary operator [87,88],

$$U(t) = |+\rangle\langle +| D[-\alpha(t)] + |-\rangle\langle -| D[\alpha(t)], \quad (9)$$

where $|\pm x\rangle$ are the eigenstates $(|g\rangle \pm |e\rangle)/\sqrt{2}$ of Pauli matrix σ_x and $D[\alpha(t)] = e^{\alpha(t)a^\dagger - \alpha^*(t)a}$ is the usual displacement operator. Therefore, the eigenstates of the effective Hamiltonian $H_{\text{eff}}(t)$ in Eq. (8) can be described as a qubit-resonator entangled state,

$$|\Psi_m(t)\rangle = \frac{1}{2} (|+\rangle D[-\alpha(t)] |m\rangle + |-\rangle D[\alpha(t)] |m\rangle), \quad (10)$$

where m represents the photon number. When the resonator is initially in the vacuum state, the ground state of $H_{\text{eff}}(t)$ in Eq. (8) can be further represented as

$$\begin{aligned} |\Psi_0(t)\rangle &= \frac{1}{2} [|+\rangle |-\alpha(t)\rangle + |-\rangle |+\alpha(t)\rangle] \\ &= \frac{1}{2} [\mathcal{N}_+ |g\rangle |\text{cat}_+(t)\rangle - \mathcal{N}_- |e\rangle |\text{cat}_-(t)\rangle]. \end{aligned} \quad (11)$$

Here, $\mathcal{N}_\pm = \sqrt{2 \pm 2 \exp[-2|\alpha(t)|^2]}$ describe the probability amplitudes of the even cat states $|\text{cat}_+(t)\rangle = [|+\alpha(t)\rangle + |-\alpha(t)\rangle]/\mathcal{N}_+$ and odd cat states $|\text{cat}_-(t)\rangle = [|+\alpha(t)\rangle - |-\alpha(t)\rangle]/\mathcal{N}_-$, respectively.

B. Generating the cat states by the STA method

To generate the cat states, we utilize the STA methods to fast generate the cat states in the subsection. It should be emphasized that the realization of the time-dependent coupling strength $\lambda_s(t)$ in Eq. (8) is needed to construct the STA passage by the transitionless tracking algorithm [49]. The coupling strength $\lambda_s(t)$ in Eq. (8) between the resonator and the qubit can be adjusted by the time variation of the squeezing parameter of $r(t)$ in the squeezing frame.

According to the theory of the transitionless tracking algorithm [49], a counterdiabatic (CD)-driving Hamiltonian,

$$H_{\text{CD}}(t) = i\dot{U}(t)U^\dagger(t) = i\sigma_x [\dot{\alpha}^*(t)a - \dot{\alpha}(t)a^\dagger] \quad (12)$$

should be added to the effective Hamiltonian $H_{\text{eff}}(t)$ in Eq. (8) to avoid nonadiabatic transitions between the instantaneous eigenstates $|\Psi_m(t)\rangle$ with eigenvalues $\xi_m(t)$ of $H_{\text{eff}}(t)$. Hence, the CD-driving Hamiltonian $H_{\text{CD}}(t)$ can accurately drive the system to evolve along the eigenstates $|\Psi_m(t)\rangle$ of $H_{\text{eff}}(t)$. It is interesting to find that adding the CD-driving Hamiltonian to the effective Hamiltonian $H_{\text{eff}}(t)$ in Eq. (8) does not change

the form of the system Hamiltonian, but only changes the effective qubit-resonator coupling strength. In this case, instead of adding the CD-driving Hamiltonian to the system, we divide the effective Hamiltonian $H_{\text{eff}}(t)$ in Eq. (8) into two parts to construct an STA passage [74],

$$\begin{aligned} H_{\text{eff}}(t) &= H'_0(t) + H'_{\text{CD}}(t), \\ H'_0(t) &= \Delta \operatorname{sech}[2r(t)]a^\dagger a + \sigma_x[\Lambda(t)a^\dagger + \Lambda^*(t)a], \\ H'_{\text{CD}}(t) &= \lambda_s(t)\sigma_x(a^\dagger + a) - \sigma_x[\Lambda(t)a^\dagger + \Lambda^*(t)a], \end{aligned} \quad (13)$$

where the Hamiltonian $H'_0(t)$ is considered as the reference Hamiltonian with an undetermined parameter $\Lambda(t)$ and $H'_{\text{CD}}(t)$ is considered as the auxiliary Hamiltonian. When the coherent amplitude $\alpha'(t)$ satisfies the conditions

$$\begin{aligned} \alpha'(t) &= \frac{\Lambda(t)}{\Delta \operatorname{sech}[2r(t)]}, \\ \dot{\alpha}'(t) &= i[\lambda_s(t) - \Lambda(t)], \end{aligned} \quad (14)$$

the Hamiltonian $H'_{\text{CD}}(t)$ in Eq. (13) can drive the system to evolve along the eigenstates $|\Psi'_m(t)\rangle$ of Hamiltonian $H'_0(t)$ in Eq. (13). By eliminating the undetermined parameter $\Lambda(t)$ in Eq. (14), we can obtain the equation of motion for the coherent-state amplitude $\alpha'(t)$,

$$\dot{\alpha}'(t) = i\{\lambda_s(t) - \alpha'(t)\Delta \operatorname{sech}[2r(t)]\}, \quad (15)$$

which indicates that the amplitude $\alpha'(t)$ of coherent state is determined by the time integration of the squeezing parameter $r(t)$, the coupling strength $\lambda_s(t)$, and the detuning Δ . Assuming the initial state of system to be $|\Psi'_0(0)\rangle = |g\rangle|0\rangle$, the evolution path along the ground state of the Hamiltonian $H'_0(t)$ in Eq. (13) is (in the squeezed frame)

$$\begin{aligned} |\Psi'_0(t)\rangle &= \frac{1}{2}[|+\rangle + |-\rangle - \alpha'(t)|+\rangle + \alpha'(t)|-\rangle] \\ &= \frac{1}{2}[\mathcal{N}'_+|g\rangle|\text{cat}'_+(t)\rangle - \mathcal{N}'_-|e\rangle|\text{cat}'_-(t)\rangle], \end{aligned} \quad (16)$$

where $\mathcal{N}'_\pm = \sqrt{2 \pm 2 \exp[-2|\alpha'(t)|^2]}$ and $|\text{cat}'_\pm(t)\rangle = [|+\rangle + \alpha'(t)|-\rangle] / \mathcal{N}'_\pm$. In the laboratory frame, the evolution state of the system is

$$|\Psi_0^{\text{lab}}(t)\rangle = U_x(t)S(t)|\Psi'_0(t)\rangle. \quad (17)$$

To obtain the target state $|\Psi'_0(t_f)\rangle$ in the laboratory frame, $U_x(t_f)S(t_f) = 1$ should be chosen, where t_f is the final time. This can be satisfied by choosing $r(t_f) = 0$ and $\Omega_c t_f = 4k\pi$ ($k = 1, 2, 3, \dots$). Thus, the final state at the time t_f is $|\Psi_0^{\text{lab}}(t_f)\rangle = |\Psi'_0(t_f)\rangle$. Note that the choice of $r(t_f)$ does not affect the amplitude of coherent state $\alpha'(t_f)$ because $\alpha'(t_f)$ relies on the time integration of $r(t)$ according to Eq. (15). By measuring the qubit in the states $|g\rangle$ and $|e\rangle$, the even and odd cat states can be further predicted by the corresponding measurement outcomes.

C. The choice of the optimized squeezing parameter

In the process of generating the target state, the choice of the time variation of the squeezing parameter $r(t)$ is crucial, which directly determines the waveforms of amplitudes $\Omega_1(t)$ and $\Omega_2(t)$ according to Eq. (6). On the one hand, for the convenience of experimental implementations, we assume that the resonator mode is initially in the vacuum state in the laboratory frame. Therefore, the initial value of parameter $\alpha'(t)$

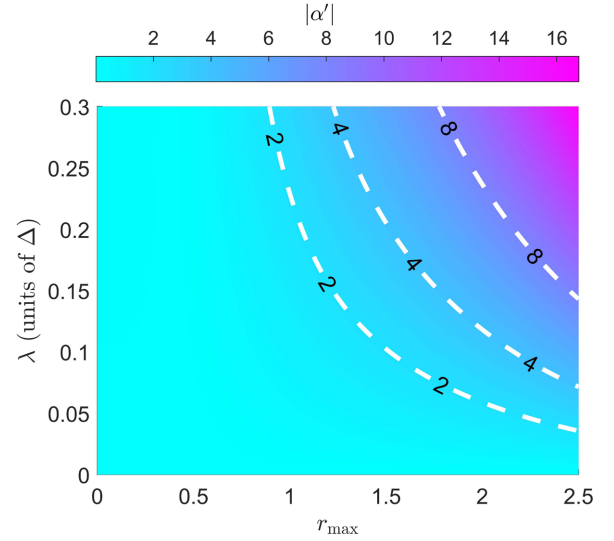


FIG. 2. The coherent-state amplitude $|\alpha'|$ versus λ/Δ and r_{max} . The parameters are chosen as $\alpha'(0) = 0$ and $t_f = 20/\Delta$.

will be $\alpha'(0) = 0$ and $r(0) = 0$ according to Eqs. (15) and (17). On the other hand, to obtain cat states in the laboratory frame, one needs to turn off the parametric drive according to Eq. (17), i.e., $r(t_f) = 0$. We should note that it is also challenging for the current technique to keep strongly squeezing a light field because the photon loss of the resonator, which is always present, destroys the essence of squeezing, i.e., two-photon correlations. Therefore, to reduce such an influence, it is better to remove the squeezing field as soon as the preparation of cat states is completed. The present method enables one to freely design the parametric drive so that the target state can be generated in the laboratory frame. In addition, pulses with finite durations are easier to realize in experiments than without. For the drivings $\Omega_1(t)$ and $\Omega_2(t)$ to have finite durations, we need the conditions $r(0) = r(t_f) = 0$ and $\dot{r}(0) = \dot{r}(t_f) = 0$.

To smoothly turn on/off the parametric drive, we choose a function $r(t) = r_{\text{max}}/\{1 + \exp[r_0 \cos(2\pi t/t_f)]\}$ to meet the requirements of drivings $\Omega_1(t)$ and $\Omega_2(t)$. The waveform of $r(t) = r_{\text{max}}/\{1 + \exp[r_0 \cos(2\pi t/t_f)]\}$ is approximately a square wave in the center of the operation time and smoothly vanishes at the boundary. The value of r_0 can be adjusted to make the initial and final values of the squeezing parameter $r(t)$ satisfy $r(0) = r(t_f) \simeq 0$ and $\dot{r}(0) = \dot{r}(t_f) \simeq 0$. Moreover, the parameter r_{max} controls the maximum value of the squeezing parameter $r(t)$. According to Eq. (15), we plot the coherent amplitude $|\alpha'|$ versus r_{max} and λ/Δ by choosing the parameters $r_0 = 10$ and $t_f = 20/\Delta$ in Fig. 2. Correspondingly, the amplitude of classical driving field may be chosen as $\Omega_c = \pi \Delta$ ($k = 5$).

In order to produce large-size cat states ($|\alpha'| > 2$), one can choose a large squeezing parameter $r(t)$ and a small coupling strength to eliminate the undesired term $H_{\text{err1}}(t)$ in Eq. (6) [74]. However, choosing a large squeezing parameter may lead to significant squeezing-induced noise in the presence of resonator loss. Therefore, it is promising to choose a small squeezing parameter $r(t)$ to generate the cat state. The detailed comparative results of squeezed-induced noise with small and large squeezing parameters are shown in Sec. IV B. Alternatively, a small squeezing parameter $r(t)$ is allowed in the

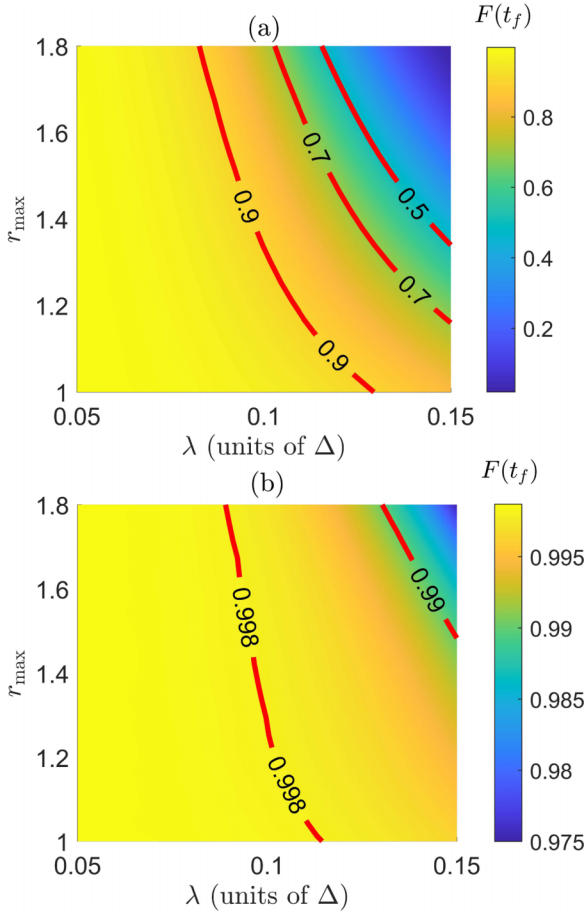


FIG. 3. (a) The final fidelity $F(t_f)$ versus λ/Δ and squeezing parameters r_{\max} without a classical driving field, i.e., $\Omega_c = 0$. (b) The final fidelity $F(t_f)$ versus λ/Δ and squeezing parameters r_{\max} with the classical driving field $\Omega_c = \pi \Delta$.

present protocol because the classical driving field Ω_c is applied to the superconducting qubit to eliminate the undesired term $H_{\text{err1}}(t)$ in Eq. (6). However, when r_{\max} is too small, generating the same amplitude $|\alpha'| > 2$ requires a strong coupling strength λ according to Fig. 2. A larger coupling strength λ increases the influence of the error term $H_{\text{err1}}(t)$. According to Eq. (7), a stronger classical drive field Ω_c is needed to eliminate the term $H_{\text{err1}}(t)$. In order to balance the requirements of small $r(t)$ and strong drive field Ω_c , we selected the proper range of r_{\max} in Fig. 3. To show the effect of the classical driving field Ω_c , we plot the fidelities $F(t_f)$ of the target state versus λ/Δ and r_{\max} with the σ_x ($\Omega_c = \pi \Delta$) drive and without the σ_x drive ($\Omega_c = 0$) in Fig. 3, where $F(t_f)$ is defined as $F(t_f) = \text{Tr}[\rho(t_f)|\Psi'_0(t_f)\rangle\langle\Psi'_0(t_f)|]$. Here, $\rho(t_f)$ represents the density operator of the system at the time t_f . As shown in Fig. 3, the fidelities $F(t_f)$ are obviously improved by adding the classical driving field on the qubit, which demonstrates that the undesired term $H_{\text{err1}}(t)$ can be effectively suppressed by the classical driving field Ω_c . In order to compare the present protocol with the scheme in Ref. [74] more clearly, we show the final fidelities $F(t_f)$ of generating the target state with the same coherent amplitude $|\alpha'| = 2$ versus the squeezing parameter r_{\max} for different amplitude of classical driving field Ω_c in Fig. 4. As shown in Fig. 4, the generation of

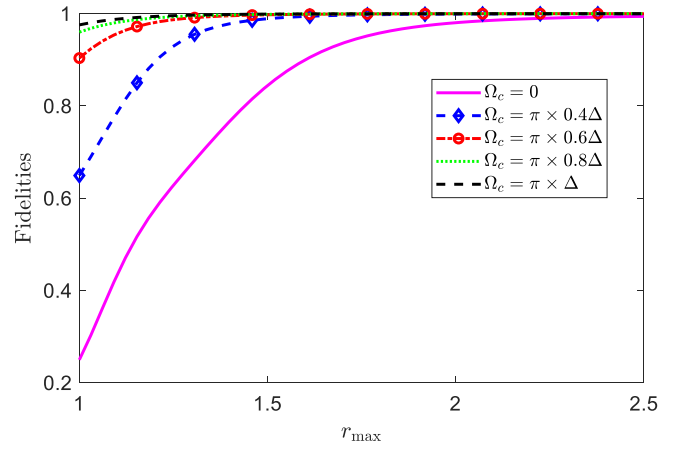


FIG. 4. The fidelities $F(t_f)$ of generating the target states with coherent amplitude $|\alpha'| = 2$ versus the squeezing parameter r_{\max} for different amplitudes of the classical driving field Ω_c .

high-fidelity cat states can occur in the wide range for r_{\max} in the present protocol ($\Omega_c \neq 0$). However, the scheme ($\Omega_c = 0$) in Ref. [74] for generating high-fidelity cat states can be generated only when the value of r_{\max} is large ($r_{\max} \geq 2.3$). Moreover, the required squeezing parameter r_{\max} for the high-fidelity cat state can be reduced with the increase in amplitude of classical driving field Ω_c . This is because the undesired term $H_{\text{err1}}(t)$ in Eq. (6) is suppressed by adding the classical driving field Ω_c instead of increasing the maximum value of squeezing parameter r_{\max} .

Next, how to choose a relatively optimized maximum value of the squeezing parameter r_{\max} is an important problem. To date, the reported amplitude of parametric drive is about 0 ~ 6 MHz in experiment [89]. In view of the experimental feasibility, we now study the choice of squeezing parameter r_{\max} . We plot the maximum of amplitudes $\max[\Omega_1(t)]$ and $\max[\Omega_2(t)]$ versus r_{\max} in Fig. 5. We can see that with the increase in r_{\max} , $\max[\Omega_1(t)]$ gradually equals to Δ , shown in Fig. 5. Compared with $\max[\Omega_1(t)]$, $\max[\Omega_2(t)]$ increases linearly with the increase in r_{\max} . This indicates that a small squeezing parameter r_{\max} can reduce the required amplitude of parametric drive. On one hand, when $\max[\Omega_2(t)]$ is smaller

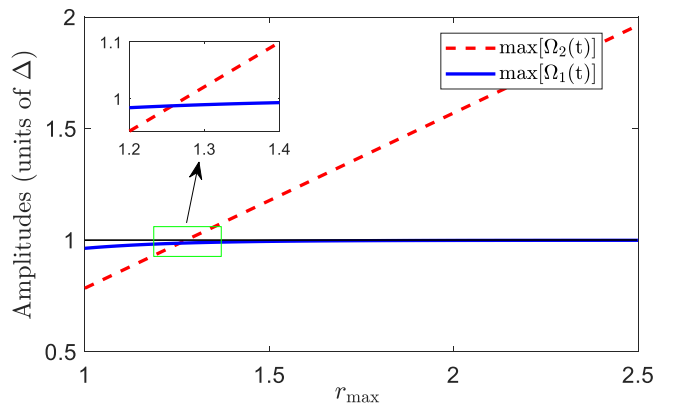


FIG. 5. The maximum amplitudes $\max[\Omega_1(t)]$ and $\max[\Omega_2(t)]$ versus r_{\max} . We choose the intersection as the optimal point $\{r_{\max} = 1.26, \max[\Omega_1(t)] = \max[\Omega_2(t)] = 0.9871 \Delta\}$.

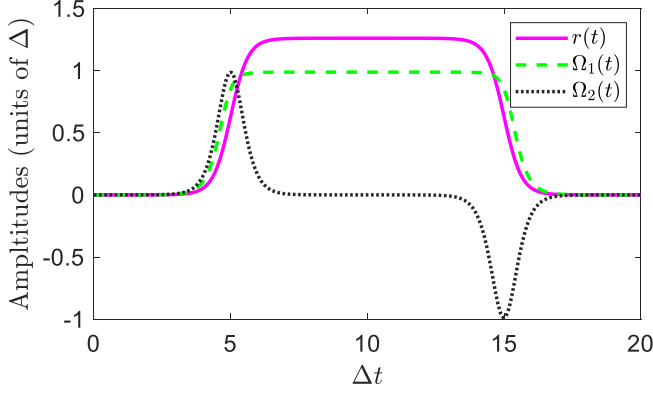


FIG. 6. The corresponding squeezing parameter $r(t)$, Rabi frequencies $\Omega_1(t)$, and $\Omega_2(t)$ versus Δt . The parameters $r_{\max} = 1.26$, $\lambda = 0.143\Delta$, $t_f = 20/\Delta$, and $\Omega_c = \pi\Delta$ are chosen.

than $\max[\Omega_1(t)]$, the required amplitude can be represented as $\max[\Omega_1(t)] = m_1\Delta$ ($m_1 < 1$). On the other hand, when $\max[\Omega_2(t)]$ is larger than Δ , the required amplitude can be represented as $\max[\Omega_2(t)] = m_2\Delta$ ($m_2 > 1$). Under the limitation of amplitude of parametric drive in experiment, the system evolution time is shorter when $\max[\Omega_2(t)]$ is smaller than $\max[\Omega_1(t)]$; and a faster evolution can alleviate the influence of dissipation on the fidelity of target state. Because the evolution time is represented as $t_f = 20/\Delta$, the evolution time t_f is shorter when the detuning Δ is larger. However, a larger Δ corresponds to a smaller r_{\max} , which requires more strong classical driving field Ω_c to suppress the term $H_{\text{err1}}(t)$ in Eq. (6). This may be a challenge in experiments due to the finite intensities of classical driving fields. Therefore, we choose an optimal squeezing parameter $r_{\max} = 1.26$ (the intersection point) as shown Fig. 5. The corresponding control pulses $\Omega_1(t)$ and $\Omega_2(t)$ and the squeezing parameter $r(t)$ versus Δt are shown in Fig. 6.

IV. NUMERICAL SIMULATIONS

In experiments, there exist some errors affecting the fidelity of the generation of the cat states. The effects of these disturbing factors are analyzed in the following.

A. Master equation

In practice, the system is inevitably coupled with the environment. Therefore, the (environment-induced) decoherence should be taken into account. The dynamics of the system is governed by the master equation [90],

$$\begin{aligned} \dot{\rho}(t) &= i[\rho(t), H(t)] + \mathcal{L}_o\rho(t), \\ \mathcal{L}_o\rho(t) &= o\rho(t)o^\dagger - \frac{1}{2}[o^\dagger o\rho(t) + \rho(t)o^\dagger o], \end{aligned} \quad (18)$$

where $\rho(t)$ is the density operator of the system and o denotes the Lindblad operator. In the system considered in this paper, there are three Lindblad operators: the spontaneous emission operator $L_\gamma = \sqrt{\gamma}|g\rangle\langle e|$, the dephasing operator $L_{\gamma\phi} = \sqrt{\gamma\phi}(|e\rangle\langle e| - |g\rangle\langle g|)$, and the resonator decay operator $L_\kappa = \sqrt{\kappa}a$.

When we map the system dynamics into the time-dependent squeezed-light frame, the master equation in

TABLE I. The corresponding physical parameters in experiment.

Physical parameters	Quantity (units of ω_q)
ω_l	1
ω_p	2
ω_c	1.001
$\max[\Omega_1(t)]$	1×10^{-3}
$\max[\Omega_2(t)]$	1×10^{-3}
Δ	1.013×10^{-3}
Ω_c	3.183×10^{-3}
λ	1.5×10^{-4}

Eq. (18) becomes

$$\begin{aligned} \dot{\rho}_s(t) &= i[\rho_s(t), H_s(t)] + \mathcal{L}_q\rho_s(t) + \mathcal{L}_c\rho_s(t), \\ \mathcal{L}_q\rho_s(t) &= \mathcal{L}(L_\gamma)\rho_s(t) + \mathcal{L}(L_{\gamma\phi})\rho_s(t), \\ \mathcal{L}_c\rho_s(t) &= (N_s + 1)\mathcal{L}(L_\kappa)\rho_s(t) + N_s\mathcal{L}(L_\kappa^\dagger)\rho_s(t) \\ &\quad - M_s\mathcal{L}'(L_\kappa)\rho_s(t) - M_s^*\mathcal{L}'(L_\kappa^\dagger)\rho_s(t), \end{aligned} \quad (19)$$

where the expressions for $\mathcal{L}(o)\rho_s$ and $\mathcal{L}'(o)\rho_s$ are

$$\begin{aligned} \mathcal{L}(o)\rho_s(t) &= o\rho_s(t)o^\dagger - \frac{1}{2}[o^\dagger o\rho_s(t) + \rho_s(t)o^\dagger o], \\ \mathcal{L}'(o)\rho_s(t) &= o\rho_s(t)o - \frac{1}{2}[oo\rho_s(t) + \rho_s(t)oo]. \end{aligned} \quad (20)$$

Here, $\rho_s(t) = S^\dagger(t)\rho(t)S(t)$ is the density operator of the system in the squeezing frame, $N_s = \sinh^2[r(t)]$ characterizes equivalent thermal noise, and $M_s = \sinh[r(t)]\cosh[r(t)]$ characterizes equivalent two-photon correlation noise in the squeezing frame.

B. Influence of the single-photon loss

When considering the single-photon loss, the coherence of the cat states may be destroyed, which leads to a statistical mixture of $|\alpha\rangle$ and $|-\alpha\rangle$ [91]. Generally, the relaxation time and the dephasing time of the superconducting qubit are about 20–60 μs [92–94]. Here, we choose the relaxation time of the qubit as $\gamma^{-1} = 40 \mu\text{s}$, and the dephasing time of the qubit as $\gamma_\phi^{-1} = 40 \mu\text{s}$. By solving the master equation in Eq. (19), we study the influence of the single-photon loss in the resonator on the fidelity of the present protocol ($r_{\max} = 1.26$) and the protocol without adding classical driving field Ω_c ($r_{\max} = 2.30$) in Fig. 7(a). In order to compare with the case in the presence of loss, we have also shown the fidelities of the target state in the absence of loss in Fig. 7(a). We can see from Fig. 7(a) that the present protocol has higher fidelity of the target state. Considering the decay time of the resonator $\kappa^{-1} = 100 \mu\text{s}$, the fidelity of target state $F(t_f)$ is 0.9539. Even when $\kappa^{-1} = 30 \mu\text{s}$, the fidelity $F(t_f)$ still reaches 0.9. To show the mechanism behind, we plot the parameters N_s and M_s versus Δt in the squeezed frame in Figs. 7(b) and 7(c), respectively. As shown in Figs. 7(b) and 7(c), the values of the parameters N_s and M_s (pink-shaded area) in the present protocol is reduced by about eight times. Thus, it is not needed for the present protocol to add a squeezing-vacuum reservoir to eliminate the influence of squeezing-induced noise, which reduces the experimental complexity. In the above numerical simulation, we have truncated the photon number $m = 60$

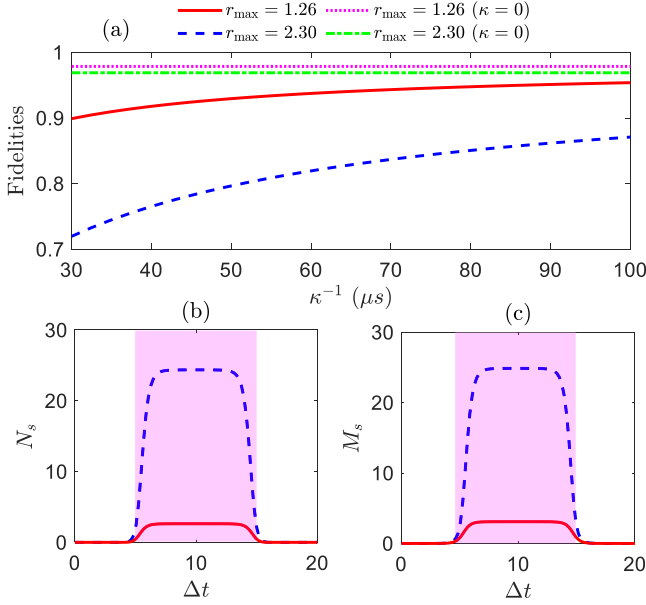


FIG. 7. (a) The fidelities $F(t_f)$ of generating the target states with coherent amplitude $|\alpha'| = 2$ versus the resonator coherent time κ^{-1} . The parameters (b) N_s and (c) M_s versus Δt in the squeezed frame. The red-solid lines represent the present protocol ($r_{\max} = 1.26$) and the blue-dashed lines represent the scheme ($r_{\max} = 2.30$) without adding the classical driving field Ω_c . The maximum amplitude of $\max[\Omega_1(t)]$ is chosen as $2\pi \times 6$ MHz, and other parameters are the same as that in Fig. 6.

of the superconducting resonator and chosen corresponding physical parameters ($\omega_q/2\pi = 6$ GHz) in experiment shown in Table I. To make sure that truncating the Hilbert space of the superconducting resonator is safe, we show the probability $P = \text{Tr}[\rho_s(t)I_q \otimes |m\rangle\langle m|]$ (I_q is identity operator of qubit) of the Fock state $|m\rangle$ in the whole evolution. As shown in Fig. 8, the Fock state $|m > 16\rangle$ is mostly never excited in the evolution, indicating that truncating the photon number at $m = 60$ is safe for numerical simulations.

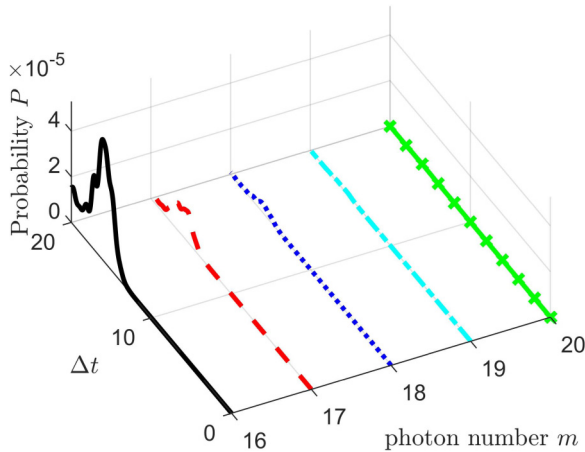


FIG. 8. The probability $P = \text{Tr}[\rho_s(t)I_q \otimes |m\rangle\langle m|]$ (I_q is identity operator of qubit) of Fock state $|m\rangle$ in the whole evolution.

To further show the quantum character of the target state, we calculate the Wigner function of the resulting cat state,

$$W(\eta) = \frac{2}{\pi} \langle D_\eta P D_{-\eta} \rangle. \quad (21)$$

Here, $D_\eta = e^{\eta a^\dagger - \eta a}$ is the displacement operator, $P = e^{i\pi a^\dagger a}$ is the parity operator, and $\langle \dots \rangle$ represents the expectation value with respect to the final cat states. By detecting the state of the superconducting qubit, the even cat state or odd cat state can be generated depended on the superconducting qubit in states $|e\rangle$ and $|g\rangle$. Here, we define the success probabilities of measuring the qubit in states $|g\rangle$ and $|e\rangle$ as $P_g = \text{Tr}[\mathcal{P}_g \rho(t_f)]$ and $P_e = \text{Tr}[\mathcal{P}_e \rho(t_f)]$ with $\mathcal{P}_g = |g\rangle\langle g| \otimes I_r$ and $\mathcal{P}_e = |e\rangle\langle e| \otimes I_r$ (I_r is identity operator of resonator), respectively. Furthermore, the fidelity of the resulting even and odd cat states can be defined as $F_{\text{even}}(t_f) = \text{Tr}[\mathcal{P}_g \rho(t_f) \mathcal{P}_g \rho'(t_f)]/P_g$ and $F_{\text{odd}}(t_f) = \text{Tr}[\mathcal{P}_e \rho(t_f) \mathcal{P}_e \rho'(t_f)]/P_e$, respectively, where $\rho'(t_f) = |\Psi'_0(t_f)\rangle\langle\Psi'_0(t_f)|$. Here, we consider the case that the decay time of the resonator $\kappa^{-1} = 100 \mu\text{s}$. By solving numerically the master equation in Eq. (19), the density operator $\rho_s(t_f) = \rho(t_f)$ of the system at the time t_f is obtained. Thus, the success probability of getting the result $|g\rangle$ and $|e\rangle$ is $P_g = 0.5030$ and $P_e = 0.4970$, respectively. Furthermore, the corresponding fidelities of even cat states and odd cat states are $F_{\text{even}}(t_f) = 0.96$ and $F_{\text{odd}}(t_f) = 0.9535$, respectively. As shown in Figs. 9(a) and 9(b), the negative quasiprobability distribution clearly displays the nonclassical quantum features of the even and odd cat states, respectively.

C. Leakage to the excited state

Up to now, we have limited the discussion to the two-level approximation of the superconducting qubit. In a realistic experiment, excitation to higher levels should be considered. The present protocol can be applied to superconducting system with different types of qubits, including transmon qubits and flux qubits [94–101]. For a superconducting transmon qubit, the typical transition frequency between neighboring levels is only 3–10 GHz. Moreover, the anharmonicity of the level spacings for a superconducting transmon qubit can be made with 100–300 MHz [96–98]. Thus, the population excited to the third level $|f\rangle$ should be considered as shown in Fig. 10(a). To illustrate this point, we investigate the fidelity of the target state by choosing the anharmonicity of the level spacings $\delta/2\pi$ from 100–1000 MHz for the present protocol, where $\delta = \omega_{eg} - \omega_{ef}$. As can be seen in Fig. 10(b), the fidelity $F(t_f)$ is 0.9216 when the value of anharmonicity of the level spacings is 300 MHz. Moreover, the typical anharmonicity of the transmon qubit is experimentally about 200 MHz. In this case, the fidelity of the target state is only 0.7716. Therefore, the transmon qubit is not the best choice to realize the present protocol. However, as shown in Refs. [99–101], the anharmonicity of a flux qubit can reach the order of gigahertz. In this case, the leakage influence of higher levels of flux qubits can be almost neglected because of its large anharmonicity. Therefore, compared with transmon qubits, flux qubits may be more efficient to implement the present protocol. The above

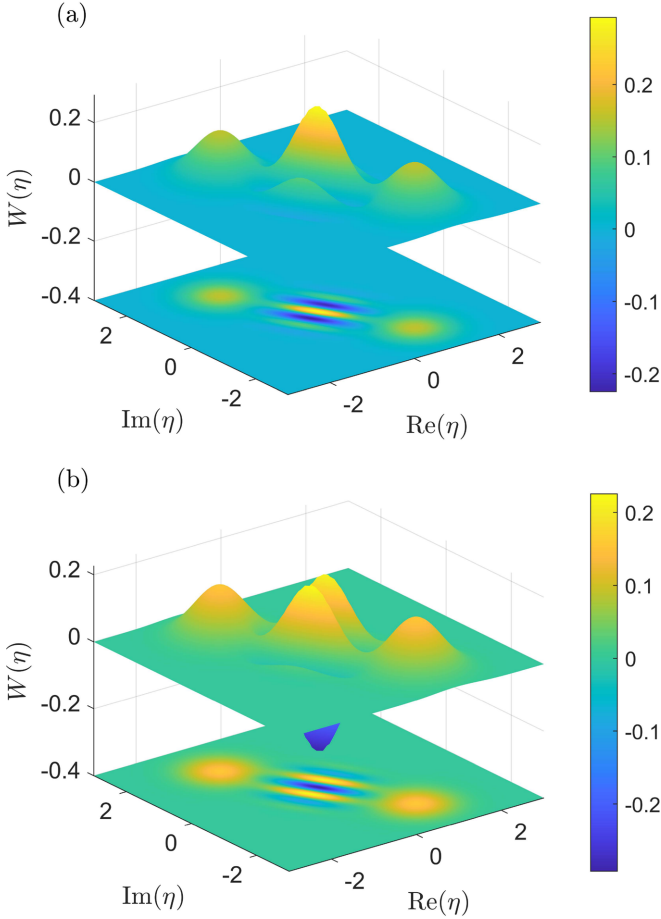


FIG. 9. (a) Wigner function of the generated even cat state at the time $t_f = 20/\Delta$ when the auxiliary qubit is in state $|g\rangle$. (b) Wigner function of the generated odd cat state at the time $t_f = 20/\Delta$ when the auxiliary qubit is in state $|e\rangle$. Considering that the relaxation time of the qubit is $\gamma^{-1} = 40 \mu\text{s}$, the dephasing time of the qubit is $\gamma_\phi^{-1} = 40 \mu\text{s}$, and the decay time $\kappa^{-1} = 100 \mu\text{s}$. The value of $\max[\Omega_1(t)]$ is chosen as $2\pi \times 6$ MHz, and other parameters are the same as that in Fig. 6.

theoretical analysis provides potential help for experimental researchers.

V. DISCUSSIONS AND CONCLUSIONS

We briefly discuss the possible extension of the protocol. As shown in Fig. 11, the superconducting qubit (circle) can be coupled to multiresonators with the capacitance or inductance. Using the same method as above in Sec. II, the effective Hamiltonian of the multiresonator system can be represented as

$$H_{\text{eff}}^h(t) = \sum_{h=1}^N \Delta \text{sech}[2r(t)] a_h^\dagger a_h + \lambda_s^h(t) \sigma_x (a_h^\dagger + a_h)/2, \quad (22)$$

with an exponentially enhanced interaction strength $\lambda_s^h(t) = \lambda_h e^{r(t)}/2$. Here, a_h (a_h^\dagger) is the annihilation (creation) operator of the h th superconducting resonator mode and λ^h denotes the coupling strength between the qubit and the h th resonator.

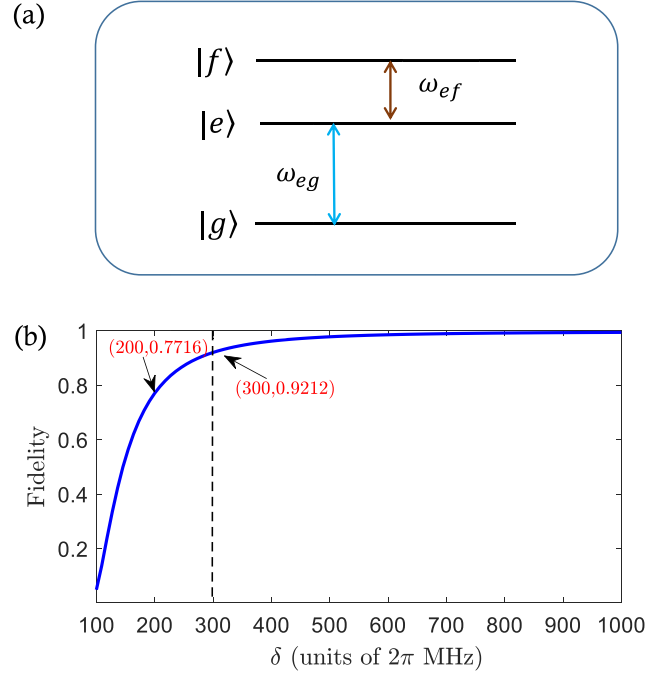


FIG. 10. (a) The level configuration of the transmon qubit. The anharmonicity of the level spacing δ can be represented as $\delta = \omega_{eg} - \omega_{ef}$, where ω_{eg} is transition frequency between levels $|e\rangle$ and $|g\rangle$ and ω_{ef} is the transition frequency between levels $|e\rangle$ and level $|f\rangle$. (b) The fidelity $F(t_f)$ versus the level spacings $\delta/2\pi$. The value of $\max[\Omega_1(t)]$ is chosen as $2\pi \times 6$ MHz, and the other parameters are the same as that in Fig. 6.

Similarly, according to Eqs. (9) and (10), the entangled states of qubit and resonators can be generated as

$$\begin{aligned} |\Psi_0(t)\rangle_h &= \frac{1}{2} [| +x\rangle | -\alpha_1(t), -\alpha_2(t), \dots, -\alpha_N(t)\rangle \\ &\quad + | -x\rangle | +\alpha_1(t), +\alpha_2(t), \dots, +\alpha_N(t)\rangle] \\ &= \frac{1}{2} [\mathcal{N}_+^h |g\rangle |\text{cat}_+^h(t)\rangle - \mathcal{N}_-^h |e\rangle |\text{cat}_-^h(t)\rangle], \end{aligned} \quad (23)$$

where $(\mathcal{N}_\pm^h)^{-1}$ are the normalization factors of the multimode entangled cat states,

$$|\text{cat}_\pm^h(t)\rangle = [| +\alpha_1(t), +\alpha_2(t), \dots, +\alpha_N(t)\rangle, \pm | -\alpha_1(t), -\alpha_2(t), \dots, -\alpha_N(t)\rangle] / \mathcal{N}_\pm^h. \quad (24)$$

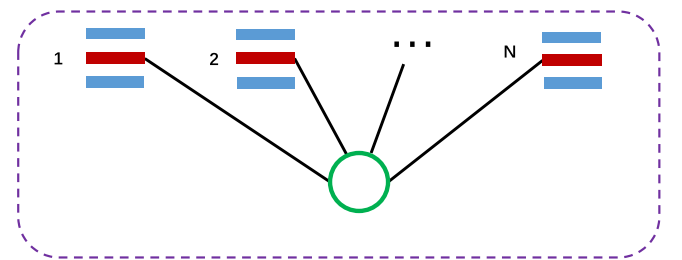


FIG. 11. Diagrammatic sketch of a possible structure for realizing the multimode cat states.

The multimode entangled cat states exhibit a great manifestation of mesoscopic superposition and entanglement, and have very wide applications in the field of quantum information and quantum communication, such as quantum metrology [40], quantum network [102], and quantum teleportation [103].

In conclusion, we have proposed an experimentally feasible protocol for generating large-size cat states of a microwave field in a weakly and parametrically driven resonator. The time-dependent parametric drive can induce adjustable coupling strength between the qubit and the resonator. By utilizing the transitionless tracking algorithm, we can design the control pulses to generate the qubit-resonator entangled states with high fidelity in the laboratory frame. Then, the even and odd cat states are predicted by the corresponding measurement outcomes of the superconducting qubit. The present protocol has several advantages as follows. First, compared with the schemes based on adiabatic and dissipation dynamics in Refs. [30,31], the present protocol by the STA method is helpful to restrain the influence of single-photon loss on the system by accelerating the evolution. Second, compared with strong squeezing scheme in Ref. [74], the present protocol assisted by an external classical driving field on the qubit can exponentially suppress the squeezing-induced noise and improve the fidelity of the generated cat states. Moreover, numerical simulations confirm the validity of the proposed protocol under experimentally available parameters. Therefore, the present protocol may provide an alternative idea for generating large-size cat states with high fidelity in superconducting quantum circuits.

ACKNOWLEDGMENTS

We acknowledge Y. Liu for helpful discussions. Y.-H.C. was supported by the Japan Society for the Promotion of Science (JSPS) KAKENHI Grant No. JP19F19028. This work was supported by the National Natural Science Foundation of China under Grants No. 11575045, No. 11874114, and No. 11674060, the Natural Science Funds for Distinguished Young Scholar of Fujian Province under Grant No. 2020J06011 and Project from Fuzhou University under Grant No. JG202001-2.

APPENDIX: POSSIBLE PHYSICAL IMPLEMENTATION OF PARAMETRIC DRIVES

As shown in Fig. 1, we consider a superconducting resonator composed of a SQUID. The Hamiltonian of the

parametric-driven resonator reads [9,17]

$$H_p = 4E_C n^2 - E_J [\Phi_{\text{ext}}(t)] \cos(\phi), \quad (\text{A1})$$

where n is the number of Cooper pairs and ϕ is the phase across the junction. Here, E_C is the resonator charging energy and E_J is the Josephson energy of the SQUID. The Josephson energy is modulated (with frequency ω_p) by the external magnetic flux $\Phi_{\text{ext}}(t)$, leading to

$$E_J [\Phi_{\text{ext}1}(t) + \Phi_{\text{ext}2}(t)] = E_J + \tilde{E}_{J1}(t) \cos(\omega_p t + \varphi_1) + \tilde{E}_{J2}(t) \cos(\omega_p t + \varphi_2), \quad (\text{A2})$$

where $\Phi_{\text{ext}1}(t)$ and $\Phi_{\text{ext}2}(t)$ are the components of the flux $\Phi_{\text{ext}}(t)$, i.e., $\Phi_{\text{ext}}(t) = \Phi_{\text{ext}1}(t) + \Phi_{\text{ext}2}(t)$. After the Taylor expansion of $\cos(\phi)$ to fourth order, we obtain

$$H_p \approx 4E_C n^2 - E_J (a - X + X^2/6) - \tilde{E}_{J1}(t) (1 - X) \cos(\omega_p t + \varphi_1) - \tilde{E}_{J2}(t) (1 - X) \cos(\omega_p t + \varphi_2), \quad (\text{A3})$$

where $X = (\phi)^2/2$.

By defining

$$n = -in_0(a - a^\dagger), \quad \phi = \phi_0(a + a^\dagger), \quad (\text{A4})$$

the quadratic time-independent part of the Hamiltonian H_p can be diagonalized, where $n_0 = [E_J/(32E_C)]^{1/4}$ and $\phi_0 = 1/2n_0$ are the zero point fluctuations. After dropping the constant terms, the Hamiltonian H_p becomes

$$H_p = \omega_c a^\dagger a - \frac{E_C}{12} (a + a^\dagger)^4 + \frac{\tilde{E}_{J1}(t)\omega_c}{4E_J} (a + a^\dagger)^2 \cos(\omega_p t + \varphi_1) + \frac{\tilde{E}_{J2}(t)\omega_c}{4E_J} (a + a^\dagger)^2 \cos(\omega_p t + \varphi_2), \quad (\text{A5})$$

where $\omega_c = \sqrt{8E_C E_J}$. When $E_C \ll E_J$, the term $\frac{E_C}{12} (a + a^\dagger)^4$ can be neglected. The whole Hamiltonian H_p can be rewritten as

$$H_p = \omega_c a^\dagger a - \frac{\tilde{E}_{J1}(t)\omega_c}{8E_J} (a + a^\dagger)^2 (e^{i\omega_p t} + e^{-i\omega_p t}) - \frac{\tilde{E}_{J2}(t)\omega_c}{8E_J} (a + a^\dagger)^2 i(e^{i\omega_p t} - e^{-i\omega_p t}), \quad (\text{A6})$$

where we have chosen $\varphi_1 = \pi$ and $\varphi_2 = 3\pi/2$. Then, moving into a rotating frame at frequency $\omega_p/2$ and neglecting all of the fast-oscillating terms, the approximate Hamiltonian under the rotating-wave approximation can be written as

$$H_p = \Delta a^\dagger a - \frac{\Omega_1(t) + i\Omega_2(t)}{2} a^2 + \text{H.c.}, \quad (\text{A7})$$

where $\Delta = \omega_c - \omega_p/2$, $\Omega_1(t) = \frac{\tilde{E}_{J1}(t)\omega_c}{4E_J}$, and $\Omega_2(t) = \frac{\tilde{E}_{J2}(t)\omega_c}{4E_J}$.

[1] Y. Makhlin, G. Schön, and A. Shnirman, *Rev. Mod. Phys.* **73**, 357 (2001).
 [2] J. Q. You and F. Nori, *Phys. Today* **58**(11), 42 (2005).
 [3] C.-P. Yang, S.-I. Chu, and S. Han, *Phys. Rev. Lett.* **92**, 117902 (2004).
 [4] Y.-x. Liu, J. Q. You, L. F. Wei, C. P. Sun, and F. Nori, *Phys. Rev. Lett.* **95**, 087001 (2005).

[5] A. Blais, J. Gambetta, A. Wallraff, D. I. Schuster, S. M. Girvin, M. H. Devoret, and R. J. Schoelkopf, *Phys. Rev. A* **75**, 032329 (2007).
 [6] Z.-L. Xiang, S. Ashhab, J. Q. You, and F. Nori, *Rev. Mod. Phys.* **85**, 623 (2013).
 [7] A. Blais, A. L. Grimsmo, S. M. Girvin, and A. Wallraff, *Rev. Mod. Phys.* **93**, 025005 (2021).

- [8] R. Barends, J. Kelly, A. Megrant, A. Veitia, D. Sank, E. Jeffrey, T. C. White, J. Mutus, A. G. Fowler, B. Campbell, Y. Chen, Z. Chen, B. Chiaro, A. Dunsworth, C. Neill, P. O'Malley, P. Roushan, A. Vainsencher, J. Wenner, A. N. Korotkov *et al.*, *Nature* **508**, 500 (2014).
- [9] X. Gu, A. F. Kockum, A. Miranowicz, Y.-X. Liu, and F. Nori, *Phys. Rep.* **718-719**, 1 (2017).
- [10] Y. Xu, W. Cai, Y. Ma, X. Mu, L. Hu, T. Chen, H. Wang, Y. P. Song, Z.-Y. Xue, Z.-Q. Yin, and L. Sun, *Phys. Rev. Lett.* **121**, 110501 (2018).
- [11] W. Ning, X.-J. Huang, P.-R. Han, H. Li, H. Deng, Z.-B. Yang, Z.-R. Zhong, Y. Xia, K. Xu, D. Zheng, and S.-B. Zheng, *Phys. Rev. Lett.* **123**, 060502 (2019).
- [12] W. Wang, L. Hu, Y. Xu, K. Liu, Y. Ma, S.-B. Zheng, R. Vijay, Y. P. Song, L.-M. Duan, and L. Sun, *Phys. Rev. Lett.* **118**, 223604 (2017).
- [13] H.-L. Huang, D. Wu, D. Fan, and X. Zhu, *Sci. China Inf. Sci.* **63**, 180501 (2020).
- [14] R. J. Schoelkopf and S. M. Girvin, *Nature* **451**, 664 (2008).
- [15] J. Clarke and F. K. Wilhelm, *Nature* **453**, 1031 (2008).
- [16] L. DiCarlo, J. M. Chow, J. M. Gambetta, L. S. Bishop, B. R. Johnson, D. I. Schuster, J. Majer, A. Blais, L. Frunzio, S. M. Girvin, and R. J. Schoelkopf, *Nature* **460**, 240 (2009).
- [17] J. Q. You and F. Nori, *Nature* **474**, 589 (2011).
- [18] P. Forn-Díaz, J. J. García-Ripoll, B. Peropadre, J.-L. Orgiazzi, M. A. Yurtalan, R. Belyansky, C. M. Wilson, and A. Lupascu, *Nat. Phys.* **13**, 39 (2017).
- [19] T. Roy, S. Kundu, M. Chand, S. Hazra, N. Nehra, R. Cosmic, A. Ranadive, M. P. Patankar, K. Damle, and R. Vijay, *Phys. Rev. Appl.* **7**, 054025 (2017).
- [20] Z. Kim, B. Suri, V. Zaretsky, S. Novikov, K. D. Osborn, A. Mizel, F. C. Wellstood, and B. S. Palmer, *Phys. Rev. Lett.* **106**, 120501 (2011).
- [21] M. Stern, G. Catelani, Y. Kubo, C. Grezes, A. Bienfait, D. Vion, D. Esteve, and P. Bertet, *Phys. Rev. Lett.* **113**, 123601 (2014).
- [22] M. A. Rol, F. Battistel, F. K. Malinowski, C. C. Bultink, B. M. Tarasinski, R. Vollmer, N. Haider, N. Muthusubramanian, A. Bruno, B. M. Terhal, and L. DiCarlo, *Phys. Rev. Lett.* **123**, 120502 (2019).
- [23] Y. Ye, Z.-Y. Ge, Y. Wu, S. Wang, M. Gong, Y.-R. Zhang, Q. Zhu, R. Yang, S. Li, F. Liang, J. Lin, Y. Xu, C. Guo, L. Sun, C. Cheng, N. Ma, Z. Y. Meng, H. Deng, H. Rong, C.-Y. Lu *et al.*, *Phys. Rev. Lett.* **123**, 050502 (2019).
- [24] Y.-H. Lin, L. B. Nguyen, N. Grabon, J. San Miguel, N. Pankratova, and V. E. Manucharyan, *Phys. Rev. Lett.* **120**, 150503 (2018).
- [25] A. Megrant, C. Neill, R. Barends, B. Chiaro, Y. Chen, L. Feigl, J. Kelly, E. Lucero, M. Mariantoni, P. J. J. O'Malley, D. Sank, A. Vainsencher, J. Wenner, T. C. White, Y. Yin, J. Zhao, C. J. Palmstrøm, J. M. Martinis, and A. N. Cleland, *Appl. Phys. Lett.* **100**, 113510 (2012).
- [26] M. Reagor, W. Pfaff, C. Axline, R. W. Heeres, N. Ofek, K. Sliwa, E. Holland, C. Wang, J. Blumoff, K. Chou, M. J. Hatridge, L. Frunzio, M. H. Devoret, L. Jiang, and R. J. Schoelkopf, *Phys. Rev. B* **94**, 014506 (2016).
- [27] M. Hofheinz, E. M. Weig, M. Ansmann, R. C. Bialczak, E. Lucero, M. Neeley, A. D. O'Connell, H. Wang, J. M. Martinis, and A. N. Cleland, *Nature* **454**, 310 (2008).
- [28] L. L. Ping, W. Li, C. J. Zhu, Y. P. Yang, and G. S. Agarwal, *Phys. Rev. Res.* **4**, 013014 (2022).
- [29] B. Vlastakis, G. Kirchmair, Z. Leghtas, S. E. Nigg, L. Frunzio, S. M. Girvin, M. Mirrahimi, M. H. Devoret, and R. J. Schoelkopf, *Science* **342**, 607 (2013).
- [30] S.-L. Ma, J.-K. Xie, and F.-L. Li, *Phys. Rev. A* **99**, 022302 (2019).
- [31] C. Leroux, L. C. G. Govia, and A. A. Clerk, *Phys. Rev. Lett.* **120**, 093602 (2018).
- [32] E. Zakka-Bajjani, F. Nguyen, M. Lee, L. R. Vale, R. W. Simmonds, and J. Aumentado, *Nat. Phys.* **7**, 599 (2011).
- [33] E. Schrödinger, *Naturwissenschaften* **23**, 823 (1935).
- [34] D. J. Wineland, *Rev. Mod. Phys.* **85**, 1103 (2013).
- [35] M. Arndt and K. Hornberger, *Nat. Phys.* **10**, 271 (2014).
- [36] I. L. Chuang, D. W. Leung, and Y. Yamamoto, *Phys. Rev. A* **56**, 1114 (1997).
- [37] W. H. Zurek, *Nature* **412**, 712 (2001).
- [38] F. Toscano, D. A. R. Dalvit, L. Davidovich, and W. H. Zurek, *Phys. Rev. A* **73**, 023803 (2006).
- [39] Z.-Y. Zhou, C. Gneiting, J. Q. You, and F. Nori, *Phys. Rev. A* **104**, 013715 (2021).
- [40] J. Joo, W. J. Munro, and T. P. Spiller, *Phys. Rev. Lett.* **107**, 083601 (2011).
- [41] C. Sánchez Muñoz, A. Lara, J. Puebla, and F. Nori, *Phys. Rev. Lett.* **121**, 123604 (2018).
- [42] W. Qin, A. Miranowicz, H. Jing, and F. Nori, *Phys. Rev. Lett.* **127**, 093602 (2021).
- [43] L. Li, C.-L. Zou, V. V. Albert, S. Muralidharan, S. M. Girvin, and L. Jiang, *Phys. Rev. Lett.* **119**, 030502 (2017).
- [44] M. Mirrahimi, Z. Leghtas, V. V. Albert, S. Touzard, R. J. Schoelkopf, L. Jiang, and M. H. Devoret, *New J. Phys.* **16**, 045014 (2014).
- [45] V. V. Albert, C. Shu, S. Krastanov, C. Shen, R.-B. Liu, Z.-B. Yang, R. J. Schoelkopf, M. Mirrahimi, M. H. Devoret, and L. Jiang, *Phys. Rev. Lett.* **116**, 140502 (2016).
- [46] Y.-H. Kang, Y.-H. Chen, X. Wang, J. Song, Y. Xia, A. Miranowicz, S.-B. Zheng, and F. Nori, *Phys. Rev. Res.* **4**, 013233 (2022).
- [47] M. Lu, Y. Xia, L.-T. Shen, J. Song, and N. B. An, *Phys. Rev. A* **89**, 012326 (2014).
- [48] D. Guéry-Odelin, A. Ruschhaupt, A. Kiely, E. Torrontegui, S. Martínez-Garaot, and J. G. Muga, *Rev. Mod. Phys.* **91**, 045001 (2019).
- [49] M. V. Berry, *J. Phys. A: Math. Theor.* **42**, 365303 (2009).
- [50] X. Chen, A. Ruschhaupt, S. Schmidt, A. del Campo, D. Guéry-Odelin, and J. G. Muga, *Phys. Rev. Lett.* **104**, 063002 (2010).
- [51] A. del Campo, *Phys. Rev. Lett.* **111**, 100502 (2013).
- [52] S. Ibáñez, X. Chen, E. Torrontegui, J. G. Muga, and A. Ruschhaupt, *Phys. Rev. Lett.* **109**, 100403 (2012).
- [53] A. Baksic, H. Ribeiro, and A. A. Clerk, *Phys. Rev. Lett.* **116**, 230503 (2016).
- [54] Y.-H. Chen, Z.-C. Shi, J. Song, Y. Xia, and S.-B. Zheng, *Phys. Rev. A* **95**, 062319 (2017).
- [55] Y.-H. Kang, Y.-H. Chen, Z.-C. Shi, B.-H. Huang, J. Song, and Y. Xia, *Phys. Rev. A* **97**, 033407 (2018).
- [56] Y.-H. Kang, Y.-H. Chen, Q.-C. Wu, B.-H. Huang, Y. Xia, and J. Song, *Sci. Rep.* **6**, 30151 (2016).
- [57] S. Ibáñez, S. Martínez-Garaot, X. Chen, E. Torrontegui, and J. G. Muga, *Phys. Rev. A* **84**, 023415 (2011).

- [58] Y.-H. Chen, Y. Xia, Q.-Q. Chen, and J. Song, *Phys. Rev. A* **89**, 033856 (2014).
- [59] Y. Liang, Q.-C. Wu, S.-L. Su, X. Ji, and S. Zhang, *Phys. Rev. A* **91**, 032304 (2015).
- [60] Y.-H. Chen, Y. Xia, Q.-Q. Chen, and J. Song, *Phys. Rev. A* **91**, 012325 (2015).
- [61] C.-P. Ho and S.-Y. Tseng, *Opt. Lett.* **40**, 4831 (2015).
- [62] Y.-H. Kang, Y.-H. Chen, Z.-C. Shi, J. Song, and Y. Xia, *Phys. Rev. A* **94**, 052311 (2016).
- [63] B.-J. Liu, Z.-H. Huang, Z.-Y. Xue, and X.-D. Zhang, *Phys. Rev. A* **95**, 062308 (2017).
- [64] B.-H. Huang, Y.-H. Kang, Y.-H. Chen, Z.-C. Shi, J. Song, and Y. Xia, *Phys. Rev. A* **97**, 012333 (2018).
- [65] Y.-H. Kang, Y.-H. Chen, Z.-C. Shi, B.-H. Huang, J. Song, and Y. Xia, *Phys. Rev. A* **97**, 042336 (2018).
- [66] H. Zhang, X.-K. Song, Q. Ai, H. Wang, G.-J. Yang, and F.-G. Deng, *Opt. Express* **27**, 7384 (2019).
- [67] P. Z. Zhao, X. Wu, T. H. Xing, G. F. Xu, and D. M. Tong, *Phys. Rev. A* **98**, 032313 (2018).
- [68] C.-Y. Guo, L.-L. Yan, S. Zhang, S.-L. Su, and W. Li, *Phys. Rev. A* **102**, 042607 (2020).
- [69] R.-H. Zheng, Y.-H. Kang, S.-L. Su, J. Song, and Y. Xia, *Phys. Rev. A* **102**, 012609 (2020).
- [70] O. Abah, R. Puebla, and M. Paternostro, *Phys. Rev. Lett.* **124**, 180401 (2020).
- [71] B.-J. Liu, X.-K. Song, Z.-Y. Xue, X. Wang, and M.-H. Yung, *Phys. Rev. Lett.* **123**, 100501 (2019).
- [72] S. Puri, S. Boutin, and A. Blais, *npj Quantum Inf.* **3**, 18 (2017).
- [73] T. Hatomura, *New J. Phys.* **20**, 015010 (2018).
- [74] Y.-H. Chen, W. Qin, X. Wang, A. Miranowicz, and F. Nori, *Phys. Rev. Lett.* **126**, 023602 (2021).
- [75] X.-Y. Lü, Y. Wu, J. R. Johansson, H. Jing, J. Zhang, and F. Nori, *Phys. Rev. Lett.* **114**, 093602 (2015).
- [76] W. Qin, A. Miranowicz, P.-B. Li, X.-Y. Lü, J. Q. You, and F. Nori, *Phys. Rev. Lett.* **120**, 093601 (2018).
- [77] Y.-H. Chen, W. Qin, and F. Nori, *Phys. Rev. A* **100**, 012339 (2019).
- [78] Y. Wang, C. Li, E. M. Sampuli, J. Song, Y. Jiang, and Y. Xia, *Phys. Rev. A* **99**, 023833 (2019).
- [79] Y. Wang, J.-L. Wu, J. Song, Z.-J. Zhang, Y.-Y. Jiang, and Y. Xia, *Phys. Rev. A* **101**, 053826 (2020).
- [80] S. Liu, D. Ran, Y.-H. Kang, Z.-C. Shi, J. Song, and Y. Xia, *Ann. Phys. (Berlin)* **532**, 2000002 (2020).
- [81] C. K. Andersen and K. Mølmer, *Phys. Rev. A* **91**, 023828 (2015).
- [82] J. R. Johansson, G. Johansson, and F. Nori, *Phys. Rev. A* **90**, 053833 (2014).
- [83] C. Macklin, K. O'Brien, D. Hover, M. E. Schwartz, V. Bolkhovsky, X. Zhang, W. D. Oliver, and I. Siddiqi, *Science* **350**, 307 (2015).
- [84] I. Siddiqi, R. Vijay, F. Pierre, C. M. Wilson, M. Metcalfe, C. Rigetti, L. Frunzio, and M. H. Devoret, *Phys. Rev. Lett.* **93**, 207002 (2004).
- [85] T. Yamamoto, K. Inomata, M. Watanabe, K. Matsuba, T. Miyazaki, W. D. Oliver, Y. Nakamura, and J. S. Tsai, *Appl. Phys. Lett.* **93**, 042510 (2008).
- [86] C. Leroux, L. C. G. Góvia, and A. A. Clerk, *Phys. Rev. A* **96**, 043834 (2017).
- [87] A. Frisk Kockum, A. Miranowicz, S. De Liberato, S. Savasta, and F. Nori, *Nat. Rev. Phys.* **1**, 19 (2019).
- [88] P. Forn-Díaz, L. Lamata, E. Rico, J. Kono, and E. Solano, *Rev. Mod. Phys.* **91**, 025005 (2019).
- [89] P. Krantz, A. Bengtsson, M. Simoen, S. Gustavsson, V. Shumeiko, W. D. Oliver, C. M. Wilson, P. Delsing, and J. Bylander, *Nat. Commun.* **7**, 11417 (2016).
- [90] M. O. Scully and M. S. Zubairy, *Quantum Optics* (Cambridge University Press, Cambridge, UK, 1997).
- [91] N. Bartolo, F. Minganti, W. Casteels, and C. Ciuti, *Phys. Rev. A* **94**, 033841 (2016).
- [92] C. Rigetti, J. M. Gambetta, S. Poletto, B. L. T. Plourde, J. M. Chow, A. D. Córcoles, J. A. Smolin, S. T. Merkel, J. R. Rozen, G. A. Keefe, M. B. Rothwell, M. B. Ketchen, and M. Steffen, *Phys. Rev. B* **86**, 100506(R) (2012).
- [93] F. Yan, S. Gustavsson, A. Kamal, J. Birenbaum, A. P. Sears, D. Hover, T. J. Gudmundsen, D. Rosenberg, G. Samach, S. Weber, J. L. Yoder, T. P. Orlando, J. Clarke, A. J. Kerman, and W. D. Oliver, *Nat. Commun.* **7**, 12964 (2016).
- [94] J. Q. You, X. Hu, S. Ashhab, and F. Nori, *Phys. Rev. B* **75**, 140515(R) (2007).
- [95] P. D. Nation, J. R. Johansson, M. P. Blencowe, and F. Nori, *Rev. Mod. Phys.* **84**, 1 (2012).
- [96] P. Krantz, M. Kjaergaard, F. Yan, T. P. Orlando, S. Gustavsson, and W. D. Oliver, *Appl. Phys. Rev.* **6**, 021318 (2019).
- [97] J. Koch, T. M. Yu, J. Gambetta, A. A. Houck, D. I. Schuster, J. Majer, A. Blais, M. H. Devoret, S. M. Girvin, and R. J. Schoelkopf, *Phys. Rev. A* **76**, 042319 (2007).
- [98] J. A. Schreier, A. A. Houck, J. Koch, D. I. Schuster, B. R. Johnson, J. M. Chow, J. M. Gambetta, J. Majer, L. Frunzio, M. H. Devoret, S. M. Girvin, and R. J. Schoelkopf, *Phys. Rev. B* **77**, 180502(R) (2008).
- [99] A. O. Niskanen, K. Harrabi, F. Yoshihara, Y. Nakamura, S. Lloyd, and J. S. Tsai, *Science* **316**, 723 (2007).
- [100] K. Inomata, T. Yamamoto, P.-M. Billangeon, Y. Nakamura, and J. S. Tsai, *Phys. Rev. B* **86**, 140508(R) (2012).
- [101] Z. H. Peng, Y.-X. Liu, J. T. Peltonen, T. Yamamoto, J. S. Tsai, and O. Astafiev, *Phys. Rev. Lett.* **115**, 223603 (2015).
- [102] C.-P. Yang, Q.-P. Su, S.-B. Zheng, and S. Han, *Phys. Rev. A* **87**, 022320 (2013).
- [103] S. J. van Enk and O. Hirota, *Phys. Rev. A* **64**, 022313 (2001).